

## A CATALOG OF NEWLY IDENTIFIED STAR CLUSTERS IN *GAIA* DR2

LEI LIU<sup>1</sup> AND XIAOYING PANG<sup>2,3,4</sup>

<sup>1</sup>*Shanghai Astronomical Observatory, Chinese Academy of Sciences, No. 80 Nandan Road, Shanghai 200030, P. R. China*

<sup>2</sup>*Xi'an Jiaotong-Liverpool University, 111 Ren'ai Road, Dushu Lake Science and Education Innovation District, Suzhou 215123, Jiangsu Province, P. R. China. Xiaoying.Pang@xjtlu.edu.cn*

<sup>3</sup>*Shanghai Institute of Technology, 100 Haiquan Road, Fengxian district, Shanghai 201418, P.R. China*

<sup>4</sup>*Shanghai Key Laboratory for Astrophysics, Shanghai Normal University, 100 Guilin Road, Shanghai 200234, P.R. China*

Submitted to ApJS

### ABSTRACT

We present the Star cluster Hunting Pipeline (SHiP) which can identify star clusters in *Gaia* DR2 data, and establish a star cluster catalog for the Galactic disk. A Friend of Friend based cluster finder method is used to identify star clusters using 5-dimensional stellar parameters,  $l$ ,  $b$ ,  $\varpi$ ,  $\mu_\alpha \cos \delta$ , and  $\mu_\delta$ . Our new catalog contains 2443 star cluster candidates identified from disk stars located within  $|b| = 25^\circ$  and with  $G < 18$  mag. An automatic isochrone fitting scheme is applied to all cluster candidates. With a combination of parameters obtained from isochrone fitting, we classify cluster candidates into three classes (Class 1, 2 and 3). Class 1 clusters are the most probable star cluster candidates with the most stringent criteria. Most of these clusters are nearby (within 4 kpc). Our catalog is cross-matched with three Galactic star cluster catalogs, [Kharchenko et al. \(2013\)](#), [Cantat-Gaudin et al. \(2018, 2019\)](#), and [Bica et al. \(2019\)](#). The proper motion and parallax of matched star clusters are in good agreement with these earlier catalogs. We discover 76 new star cluster candidates that are not listed in these 3 catalogs. The majority of these are clusters older than  $\log(\text{age}/\text{yr}) = 8.0$ , and are located in the inner disk with  $|b| < 5^\circ$ . The recent discovery of new star clusters suggests that current Galactic star cluster catalogs are still incomplete. Among the Class 1 cluster candidates, we find 56 candidates for star cluster groups. The pipeline, the catalog and the member list containing all candidates star clusters and star cluster groups have been made publicly available.

*Keywords:* star clusters: general – open clusters and associations: general – catalogs – methods: data analysis

## 1. INTRODUCTION

Star clusters in the Galactic disk are important tracers of disk structure and dynamics. Open clusters (OCs) are distributed in the disk and are (mostly) young ( $\leq 300$  Myr) and low-mass ( $< 10^3 M_{\odot}$ ; Dias et al. 2002; Piskunov et al. 2008). Perturbed by disk shocks, spiral arm passages, and encounters with molecular clouds (Spitzer 1958; Kruijssen 2012), OCs expand and disrupt at a timescale of 200 Myr - 1 Gyr (Yang et al. 2013; Pang et al. 2018). Therefore, only a small fraction of the observed OCs is older than 1 Gyr (Kharchenko et al. 2013).

In order to study the formation and evolution of open clusters, much effort has been made to compile OC catalogs, such as DAML02 (Dias et al. 2002), MWSC (Milky Way Star clusters; Kharchenko et al. 2013, K13 hereafter) and Bica et al. (2019, B19 hereafter). Based on the PPMXL proper motion catalog (Röser et al. 2010) and 2MASS photometry, MWSC developed an automated pipeline and identified 3006 star cluster objects. B19 made use of infrared photometry, and discovered several hundreds of new OC candidates in addition to those found by Kharchenko et al. (2013). The second data release (DR2) of *Gaia* (Gaia Collaboration et al. 2018) revolutionizes OC studies by providing precise proper motions of individual stars, which are very suitable for identifying star clusters in the multi-dimensional parameter space. Since its release in May 2018, several groups have published star cluster catalogs based on this archive. Cantat-Gaudin et al. (2018) developed an unsupervised membership assignment code UPMASK to search for star clusters in *Gaia* DR2. They managed to obtain parameters and members for 1229 star clusters (60 of these were new). Recently, Castro-Ginard et al. (2019) implemented a density based clustering algorithm, DBSCAN, and applied a supervised learning method (Castro-Ginard et al. 2018) to *Gaia* DR2 data. 53 new OCs were detected in a region along the direction of Galactic anti-centre and the Perseus arm. Their newly discovered OCs increase the number of known OCs in the direction of Galactic anti-center by 22% as compared to known OC populations (Kharchenko et al. 2013; Cantat-Gaudin et al. 2018, 2019, CG18+19 hereafter). Later on, Cantat-Gaudin et al. (2019) applied a “coarse-to-fine” search method and again discovered 41 new star clusters in the direction of Perseus. Therefore, all these newly discovered star clusters point out a fact that many more efforts are required to obtain a complete census of Galactic OCs. In this study, we identify star clusters in *Gaia* DR2 using our Star cluster Hunting Pipeline (SHiP). Star cluster candidates are first identified with a Friend of Friend (FoF) method. This is

directly inspired by the galaxy group finder algorithm first proposed by Yang et al. (2005). There is a long tradition of using the FoF method in cosmological studies (Davis et al. 1985). It has been successfully used for the identification of dark matter halos in cosmological simulations (Springel et al. 2001) and galaxy groups in sky survey data (Yang et al. 2007). In this method, two particles are assigned to one group if their distance is smaller than  $b_{\text{FoF}}$  (the linking length factor) times the mean separation of particles in the volume. Furthermore, the FoF method is applicable to multi-dimensional parameter spaces and does not require any prior information. At the same time, it is suitable for identifying star clusters using stellar positions, parallaxes and proper motions. Besides the FoF cluster finder, SHiP employs a full set of methods to further validate star clusters, including an automatic isochrone fitting method and a star cluster classification scheme based on a set of parameters derived during the fitting process. The efficiency of SHiP is greatly aided by parallel computation. At the same time, SHiP is capable of identifying star clusters from a huge amount of *Gaia* DR2 data without requiring any star cluster catalog as input.

This paper is organized as follows. The sample selection from *Gaia* DR2 is presented in Sec. 2. We introduce SHiP in Sec. 3, including the FoF-based star cluster finder (Sec. 3.1), the isochrone fitting method (Sec. 3.2) and the classification scheme (Sec. 3.3). In Sec. 4, we describe the general properties of the star cluster candidates (Class 1, 2, and 3), the newly discovered star clusters, and candidates of star cluster groups. Finally, a summary is presented in Sec. 5.

## 2. SAMPLE SELECTION OF *Gaia* DR2

The *Gaia* DR2 contains over one billion sources, most of which have high-precision astrometric data including parallaxes ( $\varpi$ ), proper motions ( $\mu_{\alpha} \cos \delta$  and  $\mu_{\delta}$ ), and photometry in three broad bands, the  $G$  (330 – 1050 nm),  $G_{\text{BP}}$  (330 – 680 nm) and  $G_{\text{RP}}$  (630 – 1050 nm) bands. The median uncertainties of  $\varpi$  and proper motions (without considering the systematic errors) generally increase toward faint stars. The uncertainty in  $\varpi$  is  $\sim 0.04$  mas for sources with  $G < 14$  mag, 0.1 mas for  $G \approx 17$  mag, and  $\sim 0.7$  mas for  $G \approx 20$  mag, corresponding to 0.05, 0.2 and 1.2 mas/yr of uncertainty in proper motions, respectively (Lindegren et al. 2018).

The majority of OCs are located near the Galactic plane with  $b < 20^{\circ}$  (Dias et al. 2002; Kharchenko et al. 2013; Castro-Ginard et al. 2018). Therefore, we select stars up to  $|b| = 25^{\circ}$  from *Gaia* DR2 to identify disk star clusters. At the same time, in order to exclude

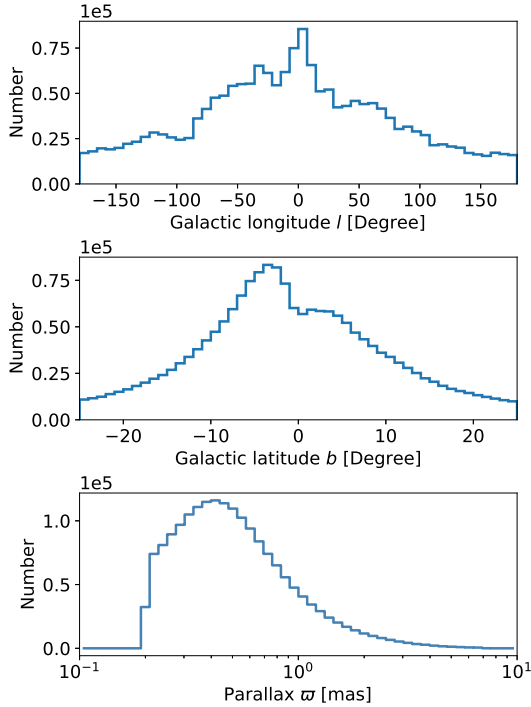


**Figure 1.** Histograms of  $l$ ,  $b$  and  $\varpi$  of stars in the primary sample.

observational artifacts due to faintness, we apply the following photometric and quality cuts:

- $G < 18$  mag,
- $\mu_\alpha \cos \delta < 30$  mas/yr,  $\mu_\delta < 30$  mas/yr,
- $0.2 \text{ mas} < \varpi < 7.0 \text{ mas}$ .

We apply the cut at  $G < 18$  mag, which is the same as the criterion used in Cantat-Gaudin et al. (2018). Since the parallax error at  $G = 18$  mag is  $\sim 0.2$  mas, we select stars with a parallax larger than 0.2 mas, which constrains our sample to a maximum distance of 5 kpc. Besides that, there are not many stars beyond 7 mas (bottom panel in Fig. 1). In total, 180,490,541 stars are retrieved for the star cluster identification. We call this set of stars the primary sample. Coordinates of stars in the primary sample are transformed from epoch 2015.5 (*Gaia* DR2) to epoch 2000, with their corresponding proper motions. Galactic longitude ( $l$ ) and latitude ( $b$ ) are calculated in the reference of epoch 2000 for a convenient cross-match with earlier catalogs (see Section 4).

In this study, we use 8 stellar parameters of stars from *Gaia* DR2 in the primary sample:  $l$ ,  $b$ ,  $\varpi$ ,  $\mu_\alpha \cos \delta$ , and  $\mu_\delta$ , and magnitudes in  $G$ ,  $G_{BP}$  and  $G_{RP}$  bands for the following procedures. Histograms of  $l$ ,  $b$ ,  $\varpi$  of the primary sample are shown in Fig. 1. Stars tend to concentrate towards the Galactic center (upper panel). The

peak of stars in the southern Galactic hemisphere is due to the Sun’s northern position off the disk (middle panel of Fig. 1, Bonatto et al. 2006; Reid et al. 2014; Gravity Collaboration et al. 2019). Parallaxes of stars in the primary sample are mostly below 2 mas (bottom panel of Fig. 1).

### 3. STAR CLUSTER HUNTING PIPELINE

#### 3.1. FoF star cluster finder

##### 3.1.1. Domain partition

SHiP adopts an FoF cluster finder to identify star clusters in the Galactic field. To facilitate this procedure, we divide the entire search volume into multiple domains. This operation enables us to carry out the cluster identification process in parallel, which greatly enhances the computational efficiency.

Stars are assigned to different domains according to their 3-D spatial coordinates ( $l, b, \varpi$ ). The specific partition strategy takes three considerations into account:

- The size of the domain should not be too large, otherwise the FoF method cannot be used due to the large surface density change of background stars in a domain from one side to the other side (see the upper and middle panels in Fig. 1). The number of stars also increases as the size becomes large, thus reducing the efficiency in the calculations.
- The size of the domain should not be too small, otherwise there will be not enough stars to carry out the identification. The size of domain should be larger than the typical size of a star cluster, so as to accommodate at least one star cluster in the domain. Besides that, we require the minimum size of the domain larger than  $\sigma_\varpi$  in parallax dimension. We set the minimum size of the domain in each dimension as  $r_{sc}$ . Here  $r_{sc} = 10$  pc is the typical scale of a star cluster (Portegies Zwart et al. 2010);  $\sigma_\varpi = 0.2$  mas is the uncertainty of parallax for  $G = 18$  mag.
- There should be sufficiently large overlapping regions between two adjacent domains along each dimension, so as to guarantee that the star cluster can be identified adequately even when it is located at the border of the domain.

According to the above three criteria, we adopt the following partitioning scheme:

- The volume is split along each dimension ( $l, b, \varpi$ ) in the following sequence: firstly the parallax  $\varpi$ ,

secondly the Galactic latitude  $b$  in the corresponding parallax range, and finally the Galactic longitude  $l$  in the corresponding ranges of the parallax and the Galactic latitude.

- A domain will be split recursively into equal parts, when it fulfills the following two criteria:
  - The size is larger than  $2r_{\text{sc}}$  in dimensions of the Galactic latitude and longitude, and is larger than  $2\sigma_{\varpi}$  in the parallax dimension.
  - The number of stars  $n$  in the domain is larger than both  $n_0/2^{k_{\text{split}}}$  and  $n_{\text{total}}/2^{k_{\text{split},\varpi}+k_{\text{split},b}+k_{\text{split},l}}$ . Here  $n_0$  is the number of stars before the split in this dimension,  $n_{\text{total}}$  is the total number of stars in the primary sample, and  $k_{\text{split}}$  is the tentative split order, which corresponds to  $k_{\text{split},\varpi}$ ,  $k_{\text{split},b}$ , and  $k_{\text{split},l}$  in the corresponding dimensions. In the current implementation, they are set to be  $k_{\text{split},\varpi}=3$ ,  $k_{\text{split},b}=3$ , and  $k_{\text{split},l}=6$ , respectively.

This partitioning process is somewhat similar to the tree method often used in cosmological simulations (Springel 2005). After carrying out the above scheme, the whole search volume is divided into 4311 domains.

- We select stars in each corresponding domain based on the 3-D spatial coordinates  $(l, b, \varpi)$  of the stars. The size of overlapping regions is  $\sigma_{\varpi}$  in the parallax dimension and  $r_{\text{sc}}$  in the  $l$  and  $b$  dimensions ( $r_{\text{sc}}$  is converted to the corresponding angle at the given distance).

### 3.1.2. Cluster identification with FoF

We use the FoF method to identify star clusters in the 5-D parameter space  $\mathbf{X} = \{l, b, \varpi, \mu_{\alpha} \cos \delta, \mu_{\delta}\}$ . A cluster is identified when the distance of one star to its nearest neighbor is smaller than the linking length factor  $b_{\text{FoF}}$  times the average distance in the domain. We normalize each of the parameters in the 5-D parameter space to the range  $(0, 1)$  so that it is scale-free. The weight of parameters

$$\mathbf{w} = (\cos b, 1, 0.5, 1, 1)/(0.2 \cos b + 0.7), \quad (1)$$

is applied to the normalized parameters. The first term,  $\cos b$ , is due to the contraction of  $l$  at a given  $b$  in spherical geometry. Since the uncertainty in the parallax is larger than that of the other parameters, we set the weight of parallax to 0.5 to reduce its influence in the cluster identification. For distance calculations we use the  $L^2$  norm (Euclidean norm). The normalization factor in the denominator guarantees that  $\sum_{i=1}^5 w_i = 5$ .

The linking length is set to  $r = b_{\text{FoF}}/N_{\text{star}}^{1/5}$ .  $b_{\text{FoF}}$  is set to 0.2, which is commonly adopted in the dark matter halo identification of cosmological simulations (Springel et al. 2001).  $N_{\text{star}}$  is the number of stars in each domain. The choice of weight and linking length together with the partitioning scheme (Sec. 3.1.1) is somewhat arbitrary, which inevitably introduces some noise and uncertainty. Therefore, the nature of these star cluster candidates identified in this way should be further confirmed by isochrone fitting and cluster classification (Sec. 3.2 and Sec. 3.3). We keep star clusters with more than 50 member stars for further merging and validation. 4885 star clusters candidates are detected within the 4311 domains in the primary sample. Some star cluster candidates appear in more than one domain. If more than 50 percent of the members in such star clusters are identical, we merge these two clusters. This merging process reduces the number of star cluster candidates to 2443.

## 3.2. Isochrone fitting Scheme

We further confirm star cluster candidates (Sec.3.1.2) by fitting their color-magnitude diagrams (CMDs) with a set of isochrones of different ages and metallicities. The reliability of star cluster candidate detections will be assessed according to the derived parameters during isochrone fitting.

### 3.2.1. The Padova Isochrones

The isochrones adopted in this work are obtained from the Padova database (Marigo et al. 2017) of stellar evolutionary tracks<sup>1</sup>. The *Gaia* DR2 passband photometric system is taken from Evans et al. (2018). We adopt a log-normal initial mass function (Chabrier 2001). A series of isochrones are generated from  $\log(t/\text{yr}) = 6.6$  to 10.13 at steps of  $\Delta(\log t) = 0.05$  for metallicities ranging from  $\log(Z/Z_{\odot}) = -2.0$  to 0.5 with steps of 0.25.

### 3.2.2. Parameters from isochrone fitting

The key to reliable isochrone fitting is the fitting function, which determines fitting accuracy. At the same time, optimization is carried out to minimize the difference between the data and the fitting function by searching the parameter space, which includes age, metallicity, distance modulus and extinction. The form of the fitting function together with the optimization method determines the fitting speed. Several studies produced isochrone fitting pipelines based on the above idea.

<sup>1</sup> [http://stev.oapd.inaf.it/cgi-bin/cmd\\_3.0](http://stev.oapd.inaf.it/cgi-bin/cmd_3.0)

Perren et al. (2015) used the Bayesian approach and genetic algorithm to maximize the likelihood of the fitted parameters. Another optimization function is the residual hyper-surface (the discrepancy between the observed and simulated Hess diagrams) used by Bonatto (2019), which minimizes the function with simulated annealing.

Automated isochrone fitting of 2443 star cluster candidates requires an efficient fitting scheme, which at the same time provides good accuracy. To fulfill these requirements, we propose the following fitting function:

$$\bar{d}^2 = \sum_{k=1}^n |\mathbf{x}_k - \mathbf{x}_{k,nn}|^2/n. \quad (2)$$

Here  $\mathbf{x}_k = [G_k + \Delta_G, (G_{\text{BP}} - G_{\text{RP}})_k + \Delta_{G_{\text{BP}}-G_{\text{RP}}}]$  is the position of the  $k$ -th star in the CMD with absolute magnitudes.  $\mathbf{x}_{k,nn}$  is the  $k$ -th star's corresponding nearest neighboring point in the isochrone table. Four parameters are obtained from isochrone fitting:  $\Delta_G$  (distance modulus in  $G$  magnitude),  $\Delta_{G_{\text{BP}}-G_{\text{RP}}}$  (color excess  $E(G_{\text{BP}} - G_{\text{RP}})$ ), metallicity  $Z$  and age  $t$ . We minimize  $\bar{d}^2$ , the mean square distance between cluster stars and their closest neighboring points in the isochrone. This approach is easy to implement and sensitive to the discrepancy between isochrones and the actual data. The nearest neighbor in the isochrone can be easily found with the  $k$ -D Tree method, which facilitates speeding up the fitting process of the 770 isochrones (each isochrone contains over 1500 points) for each star cluster candidate. Besides, the optimization of  $\bar{d}^2$  is easily carried out by the Nelder-Mead algorithm (Nelder & Mead 1965) provided by the “scipy” package.

The main sequence (MS) is significantly broadened at the faint end, due to the uncertainty in brightness of faint stars at  $G > 17$  mag ( $\delta G \sim 0.072$  mag), which is three times larger than those with  $G < 17$  mag ( $\delta G \sim 0.023$  mag). Approximately 30% of the members among our identified clusters are fainter than  $G = 17$  mag, which greatly affects the quality of the isochrone fitting. Therefore, we restrict the isochrone fitting to stars brighter than  $G = 17$  mag. This treatment reduces the number of stars in the fitting by approximately 50 percent, but substantially improves the quality of the fits.

### 3.3. Star cluster classification

In order to evaluate the reliability of star cluster candidates detections using the FoF cluster finder, we carry out a classification based on parameters obtained from isochrone fitting. Because of observational uncertainties, there is no unique parameter that can represent the reliability of a star cluster detection accurately. Instead, a combination of several parameters can be used to min-

imize the influence of the uncertainties. Therefore, we classify candidates based on the following parameters.

- $\bar{d}^2$ : the average square of the distance between cluster stars and an isochrone. It can be used to estimate the fitting quality. A small value of  $\bar{d}^2$  represents a good isochrone fitting.

- $r_n$ : the narrowness of the MS in the CMD. This parameter is used to distinguish real star clusters from false detections. For example, a real cluster tends to show a narrow MS, while an artifact might be very broad. The narrowness of the MS is defined as  $r_n = |v_1/v_2|$ . Here  $v_1$  and  $v_2$  are the two eigenvalues of the covariance matrix  $\mathbf{M}$  of the distribution of stars in the CMD, with  $|v_1| < |v_2|$ . The covariance matrix  $\mathbf{M}$  is defined as:

$$\mathbf{M} = \begin{pmatrix} \overline{x_i x_i} & \overline{x_i y_i} \\ \overline{x_i y_i} & \overline{y_i y_i} \end{pmatrix}. \quad (3)$$

Here  $x_i = (G_{\text{BP}} - G_{\text{RP}})_i - \overline{G_{\text{BP}} - G_{\text{RP}}}$ ,  $y_i = G_i - \overline{G}$ . According to the definition of  $r_n$ , a smaller value corresponds to a narrower MS. There is a certain degree of degeneration between  $r_n$  and  $\bar{d}^2$ . A star cluster with a good isochrone fitting usually has small values of both  $\bar{d}^2$  and  $r_n$ .

- $n_{G < 17}$ : the number of bright stars with  $G < 17$  mag included in the isochrone fitting. Since photometric uncertainty broadens the MS at the faint end,  $n_{G < 17}$  eliminates contamination and guarantees the quality of the selected star cluster candidates. Inevitably, this parameter will make our results biased towards relatively nearby clusters that contain a sufficient number of bright stars for isochrone fitting.

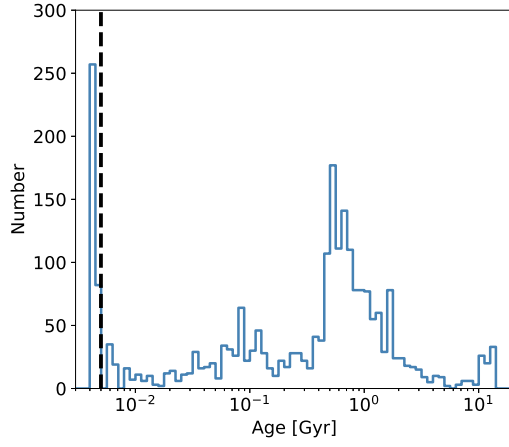
- $t_{\text{age}}$ : the age of star clusters derived from isochrone fitting. The starting age of the Padova isochrones is  $t = 4$  Myr ( $10^{6.6}$  yr). We plot the age distribution of star cluster candidates in Fig. 2. The interpretation of the ages of the peak below 5 Myr (Fig. 2) are highly uncertain since it approaches the lowest limit of the isochrone ages. To ensure a reliable cluster classification, we consider only star cluster candidates with ages older than 5 Myr, which yield better fitting results.

According to the above four criteria, we divide the 2443 star cluster candidates into 3 classes:

- Class 1:  $n_{G < 17} \geq 50$ ,  $t_{\text{age}} > 5$  Myr,  $r_n < 0.1$ ,  $\bar{d}^2 < 0.05$ ;
- Class 2:  $n_{G < 17} \geq 50$ ,  $t_{\text{age}} > 5$  Myr,  $r_n < 0.1$ ;
- Class 3: all other cases.

The numbers of star cluster candidates in each group are: Class 1: 569 (23.3%); Class 2: 127 (5.2%); and Class 3: 1747 (71.5%).  $n_{G < 17} \geq 50$  restricts Class 1

**Figure 2.** The distribution of isochrone fitted ages of star clusters. The black dashed line represents the 5 Myr age cut.



and 2 to nearby star clusters, mainly within 4 kpc. The classification of star cluster candidates is influenced by the performance of our pipeline in the identification process, and should not be directly linked to the physical existence of those star cluster candidates. According to our analysis, members of Class 1 are likely star cluster candidates. Class 2 and 3 are candidates that need further confirmation. However, genuine star clusters may exist among the members of Class 2 and Class 3 (see Sec. 4.2). General parameters for all 2443 candidates are presented in Tab. 1.



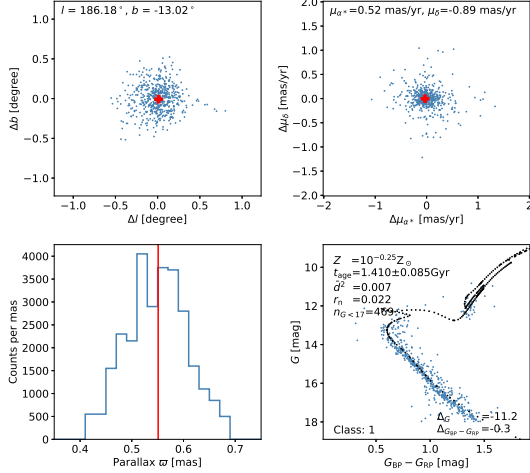
**Table 1.** Parameters of the 2443 star cluster candidates identified by SHiP in this work. The position, parallax and proper motion of each star cluster are calculated as the average value of all cluster members with one sigma dispersion indicated. The radius  $r_{\max}$  is defined as the maximum distance of cluster members to the average position. For convenience, the corresponding IDs in K13, CG18+19 and B19 are also listed ( $-1$  means unmatched). All IDs start with 0 and correspond to the line number in the catalog (not the MWSC number as in K13). For CG18+19, IDs in the ranges  $0 - 1228$  and  $1229 - 1274$  correspond to star clusters in [Cantat-Gaudin et al. \(2018\)](#) and [Cantat-Gaudin et al. \(2019\)](#), respectively. For convenience, the names of the matched star clusters in CG18+19 are also presented. Uncertainties of age and metallicity are estimated as half a step in the isochrone table (see Sec. 3.2.1 for more details). These are 6% ( $10^{\frac{1}{2}\Delta(\log t/\text{yr})}$ ) for ages and 0.125 for metallicities. A machine readable table is available online, see data/cat\_all.txt in the github repository for a full version.

FoF ID	$l$ (deg)	$b$ (deg)	$r_{\max}$ (deg)	$\varpi$ (mas)	$\mu_{\alpha} \cos \delta$ (mas/yr)	$\mu_{\delta}$ (mas/yr)	$n_{\text{tot}}$	$t_{\text{age}}$ (Gyr)	$Z$ ( $\log \frac{Z}{Z_{\odot}}$ )	Class	K13 ID	CG18+19 ID	B19 ID	Name
0	$186.181 \pm 0.182$	$-13.025 \pm 0.173$	0.817	$0.549 \pm 0.058$	$0.516 \pm 0.252$	$-0.888 \pm 0.221$	567	$1.41 \pm 0.08$	-0.250	1	352	687	5076	NGC_1817
1	$184.719 \pm 0.120$	$-13.510 \pm 0.077$	0.470	$0.359 \pm 0.052$	$0.355 \pm 0.224$	$-2.500 \pm 0.220$	135	$1.32 \pm 0.08$	0.000	1	-1	-1	5047	-
2	$226.034 \pm 0.110$	$-16.126 \pm 0.116$	0.461	$0.252 \pm 0.039$	$-0.538 \pm 0.237$	$1.975 \pm 0.282$	384	$1.38 \pm 0.08$	0.250	1	576	708	6219	NGC_2204
3	$239.472 \pm 0.069$	$-18.018 \pm 0.062$	0.331	$0.257 \pm 0.048$	$-1.261 \pm 0.151$	$5.493 \pm 0.164$	361	$3.39 \pm 0.20$	0.000	1	625	713	6569	NGC_2243
4	$259.574 \pm 0.073$	$-14.278 \pm 0.089$	0.384	$0.258 \pm 0.040$	$-1.476 \pm 0.200$	$2.740 \pm 0.255$	330	$2.69 \pm 0.16$	0.000	1	917	651	7005	Melotte_66
5	$292.316 \pm 0.216$	$-12.736 \pm 0.129$	0.559	$0.506 \pm 0.026$	$-6.873 \pm 0.177$	$1.425 \pm 0.215$	171	$3.16 \pm 0.19$	0.000	1	-1	-1	-1	-
6	$325.553 \pm 0.032$	$-17.569 \pm 0.035$	0.118	$0.242 \pm 0.031$	$-5.552 \pm 0.208$	$-4.683 \pm 0.316$	126	$10.70 \pm 0.64$	-2.000	3	2106	-1	9172	-
7	$0.069 \pm 0.027$	$-17.299 \pm 0.031$	0.133	$0.280 \pm 0.054$	$0.900 \pm 0.379$	$-2.391 \pm 0.401$	206	$0.85 \pm 0.05$	-2.000	3	2420	-1	10	-
8	$5.617 \pm 0.034$	$-14.071 \pm 0.069$	0.367	$0.281 \pm 0.063$	$-2.958 \pm 0.399$	$-1.410 \pm 0.429$	176	$0.0040 \pm 0.0002$	0.500	3	2412	-1	338	-
9	$8.793 \pm 0.054$	$-23.268 \pm 0.054$	0.265	$0.341 \pm 0.120$	$-3.412 \pm 0.404$	$-9.270 \pm 0.366$	1798	$12.90 \pm 0.77$	-2.000	1	2506	-1	473	-

**Table 2.** Summary of the total number of cross matched star clusters with K13, CG18+19 and B19.

Catalog	Class			Total
	1	2	3	
K13	439	72	391	902
CG18+19	430	51	233	714
B19	444	62	370	876

**Figure 3.** The distributions of position, proper motion, parallax and the CMD of a typical Class 1 star cluster candidate that cross-matched with CG18+19. The positions and proper motions of cluster members are plotted as offsets to the mean value of all members (the average position and proper motion of members are presented in the upper left corner of the corresponding panel). Blue dots represent cluster members. Red crosses and lines demonstrate the corresponding mean position, proper motion and parallax obtained from CG18+19. The black dotted curve in the CMD panel is the best-fitting isochrone. The fitted parameters are presented in the same panel. A detailed description of these parameters is given in Sec. 3.2.2.



## 4. STAR CLUSTER CANDIDATES

### 4.1. General properties

Among all 2443 star cluster candidates, those in Class 1 are likely genuine star clusters which are mostly located within 4 kpc. For these cluster candidates, a clear over-density is seen in the spatial and proper motion distributions of cluster members (upper panels in Fig. 3). Member stars form a narrow MS in the CMD (bottom-right panel in Fig. 3). On the contrary, star cluster candidates in Class 2 are more diffuse in distri-

**Figure 4.** The distributions of position, proper motion, parallax and the CMD of member stars of a typical Class 2 star cluster candidate. The symbols and colors are identified to those in Fig. 3.

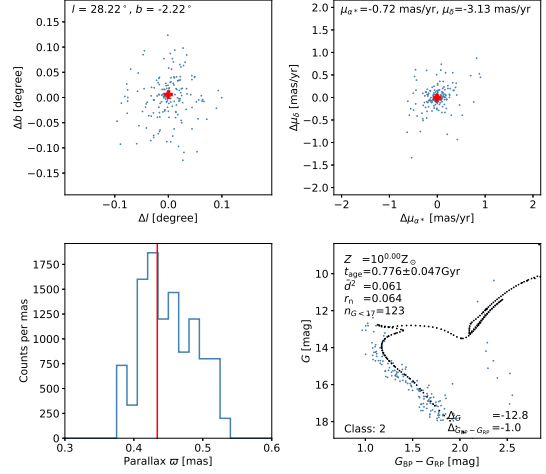
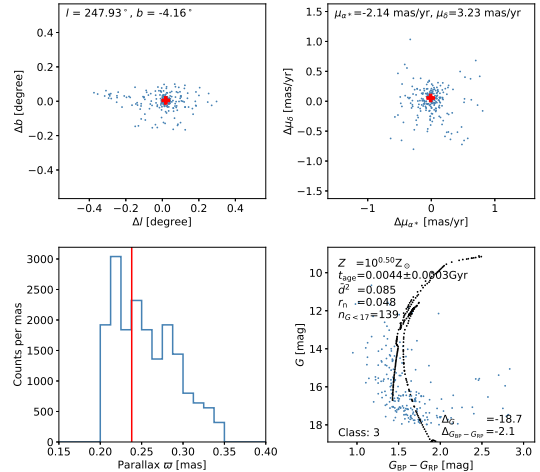


**Figure 5.** The distributions of position, proper motion, parallax and the CMD of member stars of a typical Class 3 star cluster candidate. The symbols and colors are identified to those in Fig. 3.



butions of position, proper motion and CMD (Fig. 4)<sup>2</sup>. Note that the appearance of a few outliers may have biased the fitting results. There is no standard criteria to automatically exclude stars from star cluster candidates. This can be done manually for individual clusters. For example, after removing the few faint red stars in Fig. 4 ( $G_{\text{BP}} - G_{\text{RP}} > 2 \text{ mag}$ , and  $G > 14 \text{ mag}$ ), the fitted age changes from 776 Myr to 380 Myr, and the metallic-

<sup>2</sup> The 4-panel diagrams (Fig. 3, 4 and 5) together with the member list of all 2443 candidates are available in the github repository of this work.



ity changes from  $\log(Z/Z_{\odot}) = 0$  to  $\log(Z/Z_{\odot}) = -0.75$ . Therefore, a followup study of the Class 2 and Class 3 star cluster candidates may require visual inspection of their CMDs.

Although cluster members of Class 3 candidates are widely scattered in the CMD, without a clear MS (Fig. 5), there is still a clear and notable concentration of stars in the  $(l, b)$  and proper motions (upper panels in Fig. 5). The candidate shown in Fig. 5 is a cluster cross-matched with the CG18+19 catalog, which implies that there are genuine star clusters in Class 3 that deserve further investigation.

#### 4.2. Cross-match with previous catalogs

We cross-match our identified star cluster candidates with three previously published catalogs: K13, CG18+19 and B19, so as to verify the reliability of our catalog. K13 is compiled by Kharchenko et al. (2013), and contains 3006 objects with 2MASS photometry; CG18+19 is a *Gaia* DR2 based catalog, which combines 1229 objects in Cantat-Gaudin et al. (2018) and 46 objects in Cantat-Gaudin et al. (2019). B19 is a multi-band catalog with 10978 entries composed of Galactic star clusters, stellar associations and candidates in Bica et al. (2019). To keep the same volume, star clusters with  $|b| > 25^{\circ}$  are excluded, which yields 2941 (K13), 1270 (CG18+19) and 10464 (B19) star clusters in the three catalogs for the following cross-matches, respectively.

A star cluster candidate in our catalog is cross-matched after comparison of their radii in the other catalogs. For our candidates, the radius  $r_{\text{FoF}}$  is defined as the maximum cluster-centric distance of members. We adopt the average position of members as the cluster center. For K13 we use  $r_2$ , which is defined as the projected distance from the cluster centre where the surface density of cluster members is equal to the average surface density of the surrounding field (Kharchenko et al. 2012). For CG18+19,  $r_{50}$ , the radius which contains half the number of members, is adopted. For B19, we use the major axis of the cluster. To obtain appropriate matching criteria, we test a variety of methods using our catalog and CG18+19, such as,  $d < (r_{\text{FoF}} + r_{\text{REF}})$ ,  $d < \max(r_{\text{FoF}}, r_{\text{REF}})$ , etc. Here  $d$  is the angular distance between the centers of the two clusters.  $r_{\text{REF}}$  is the radius of the star cluster provided in the reference catalog. We further exclude artificial cross-matches that may occur when two clusters are located along nearly the same line of sight, by comparing their radii and angular separations, and the parallaxes. After our investigation, a star cluster candidate in our catalog is regarded as cross-matched with the cluster in the other

catalogs when the angular distance between their centers is smaller than any of their radii,  $d < \min(r_{\text{FoF}}, r_{\text{REF}})$ . This cross-matching criterion yields the lowest artificial visual overlapping fraction and provides a reasonable matching number. 430 star clusters candidates of Class 1 are cross-matched with CG18+19, 3 clusters among these exhibit visual overlap<sup>3</sup>; for other criteria:  $d < (r_{\text{FoF}} + r_{\text{REF}})$  and  $d < \max(r_{\text{FoF}}, r_{\text{REF}})$ , artificial visual overlaps increase to 16 (456 cross-matched) and 13 (451 cross-matched), respectively. In Tab. 1, we present the corresponding ID for each matched cluster.

The cross-matched results are summarized in Tab. 2. Overall, 902, 714 and 876 star cluster candidates are matched with K13, CG18+19 and B19, respectively.

There is no difference in the metallicity and age distribution between the cross-matched and unmatched star cluster candidates. Generally, unmatched cluster candidates are much further away from the Sun than the cross-matched. Since CG18+19 is completely based on *Gaia* DR2 data, the corresponding parameters are more consistent with our catalog. Among the 1270 star clusters ( $|b| < 25^{\circ}$ ) in CG18+19, over half are identified by SHiP. We use CG18+19 to validate parameters of cross-matched star clusters derived from our pipeline.

The mean values of position, proper motion and parallax from CG18+19 are plotted as red crosses and lines in Fig. 3, 4 and 5, which are consistent with the average value from our pipeline. Fig. 6 shows the discrepancy of proper motions and parallax of matched clusters compared to CG18+19 (blue dashed histograms). The peak around 0.1 mas/yr of the proper motions is smaller than the typical spread in the proper motions of the cluster stars ( $\sim 1.0$  mas/yr). Similarly, the differences of the parallax are well within 0.1 mas, which is smaller than the uncertainty of the parallax at  $G \sim 18$  mag (0.2 mas). Very few star clusters have discrepancies in proper motion and parallax that are larger than 1 mas/yr and 10 mas, respectively. Generally, the discrepancy distribution of the best fitted Class 1 candidates (red histograms in Fig. 6) shows no difference for all matched samples (blue dashed histograms).

Given the same cluster, its number of members brighter than  $G = 17$  mag (parameter  $n_{G < 17}$ ) is larger when it is nearer. Therefore, among the 714 matched star cluster candidates with CG18+19, Class 1 candidates are primarily star clusters within 4 kpc (larger

<sup>3</sup> The IDs of the three visual overlaps are 380, 2129 and 2281 in our catalog. However, their cross-match with K13 or B19 still cannot be excluded (the parallax information provided by K13 does agree not well with the *Gaia* catalog. B19 provides no parallax information).

**Figure 6.** The discrepancy distributions of proper motions and parallaxes for the matched star clusters, for our identifications and those of CG18+19. Blue dashed histograms and red solid histograms correspond to all matched clusters and those classified as Class 1, respectively.

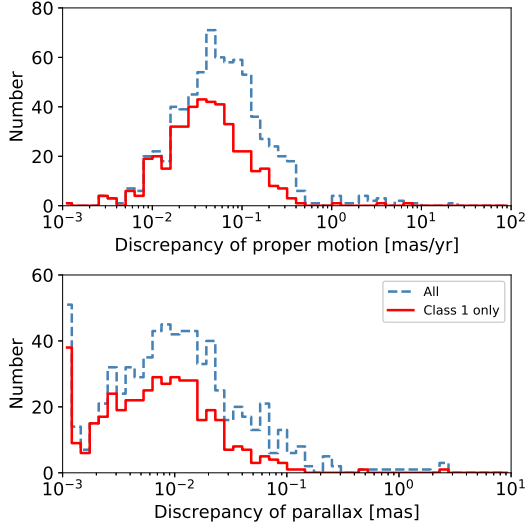


**Figure 7.** The distributions of parallax (upper panel) and age (lower panel) of cross-matched star clusters with CG18+19. Red solid, cyan dotted and blue dashed histograms represent star cluster candidates in Class 1, 2, and 3, respectively.

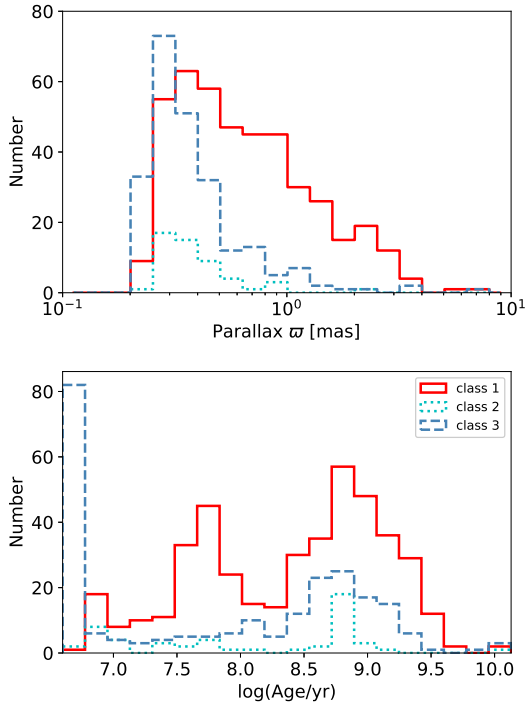
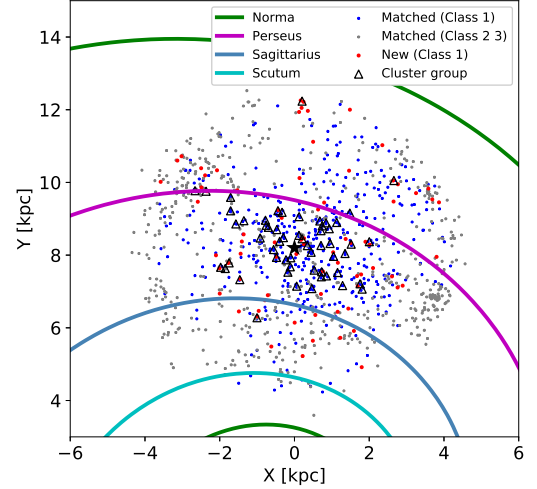


**Figure 8.** The distributions of matched and new star cluster candidates of different classes in the Galactic X-Y plane with indication of spiral arms. The positions (mean position of cluster members) of identified cluster group candidates are also presented.



value of parallax; see the upper panel in Fig. 7), and on average slightly closer than clusters in Class 2 and Class 3 (Fig. 8).

At the same time, the age distributions among the three classes (bottom panel in Fig. 7) are distinct. Class 1 clusters show two populations. The young population has a broad peak around  $\log(\text{age}/\text{yr}) \sim 7.8$  and the old population at  $\log(\text{age}/\text{yr}) \sim 8.8$ . Class 2 only has a dominant old population at  $\log(\text{age}/\text{yr}) \sim 8.8$ . Similar to Class 1 and 2, there is also an old population at  $\log(\text{age}/\text{yr}) \sim 8.8$  in Class 3. Additionally, Class 3 contains a very young population at  $\log(\text{age}/\text{yr}) < 6.8$ , which does not exist in other two classes. This is due to our age cut at 5 Myr for Class 1 and 2. On the other hand, studies of solar neighborhood star clusters did find an excess of young star clusters with ages  $\leq 9$  Myr (Bonatto & Bica 2011). Therefore, the young cluster candidates in Class 3 deserve further investigation. Old star clusters with  $\log(\text{age}/\text{yr}) \sim 8.8$  have a prominent MS turn-off in the CMD, enabling reliable isochrone fitting. At the age of  $\log(\text{age}/\text{yr}) \sim 7.8$  (Class 1), the radiation of young massive stars has already dispersed the parent molecular clouds. Therefore, such clusters are free from differential reddening and have a relatively narrow MS that enables reliable isochrone fitting with our pipeline. In the discussion below, we will focus on the most probable cluster candidates in Class 1.

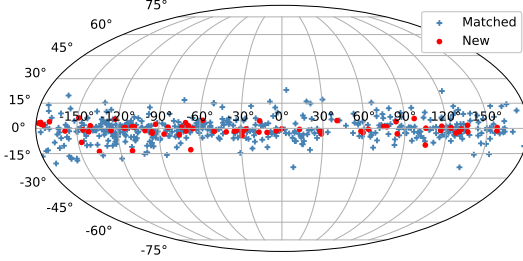
#### 4.3. New star cluster candidates in Class 1

A total of 76 star cluster candidates classified as Class 1 are not present in any of the three earlier catalogs, which accounts for 13.6% of the total number of clus-

**Table 3.** The 76 new star cluster candidates classified as Class 1. A machine readable table is available online; see data/cat\_new.txt in the github repository for a full version.

FoF ID	$l$	$b$	$r$	$\varpi$	$\mu_{\alpha \cos \delta}$	$\mu_{\delta}$	$n_{\text{tot}}$	$t_{\text{age}}$	$Z$
	(deg)	(deg)	(deg)	(mas)	(mas/yr)	(mas/yr)		(Gyr)	( $\log \frac{Z}{Z_{\odot}}$ )
5	$292.316 \pm 0.216$	$-12.736 \pm 0.129$	0.559	$0.506 \pm 0.026$	$-6.873 \pm 0.177$	$1.425 \pm 0.215$	171	$3.16 \pm 0.19$	0.000
58	$264.972 \pm 0.232$	$-2.881 \pm 0.093$	0.768	$0.524 \pm 0.034$	$-5.813 \pm 0.286$	$5.063 \pm 0.251$	482	$0.02 \pm 0.00$	0.250
145	$343.191 \pm 0.068$	$-2.218 \pm 0.048$	0.208	$0.518 \pm 0.049$	$-2.103 \pm 0.251$	$-5.424 \pm 0.230$	264	$0.98 \pm 0.06$	0.250
198	$234.945 \pm 0.107$	$-1.276 \pm 0.039$	0.347	$0.310 \pm 0.041$	$-1.972 \pm 0.534$	$2.311 \pm 0.589$	147	$0.54 \pm 0.03$	-0.750
273	$333.632 \pm 0.028$	$-0.346 \pm 0.030$	0.101	$0.362 \pm 0.036$	$-2.346 \pm 0.365$	$-4.109 \pm 0.289$	97	$1.48 \pm 0.09$	-0.750
282	$355.798 \pm 0.032$	$-1.447 \pm 0.031$	0.095	$0.335 \pm 0.025$	$-0.027 \pm 0.244$	$-0.994 \pm 0.299$	75	$0.69 \pm 0.04$	0.500
321	$57.818 \pm 0.047$	$-1.706 \pm 0.043$	0.151	$0.423 \pm 0.049$	$-0.360 \pm 0.187$	$-3.504 \pm 0.197$	132	$0.68 \pm 0.04$	0.500
386	$250.132 \pm 0.135$	$0.927 \pm 0.079$	0.315	$0.255 \pm 0.026$	$-2.534 \pm 0.378$	$3.076 \pm 0.502$	193	$0.58 \pm 0.03$	0.250
403	$286.748 \pm 0.048$	$0.721 \pm 0.038$	0.172	$0.367 \pm 0.031$	$-6.939 \pm 0.345$	$3.019 \pm 0.255$	164	$0.0060 \pm 0.0004$	0.500
589	$237.710 \pm 0.067$	$5.499 \pm 0.040$	0.212	$0.304 \pm 0.033$	$-1.398 \pm 0.172$	$0.536 \pm 0.174$	87	$0.76 \pm 0.05$	-0.750

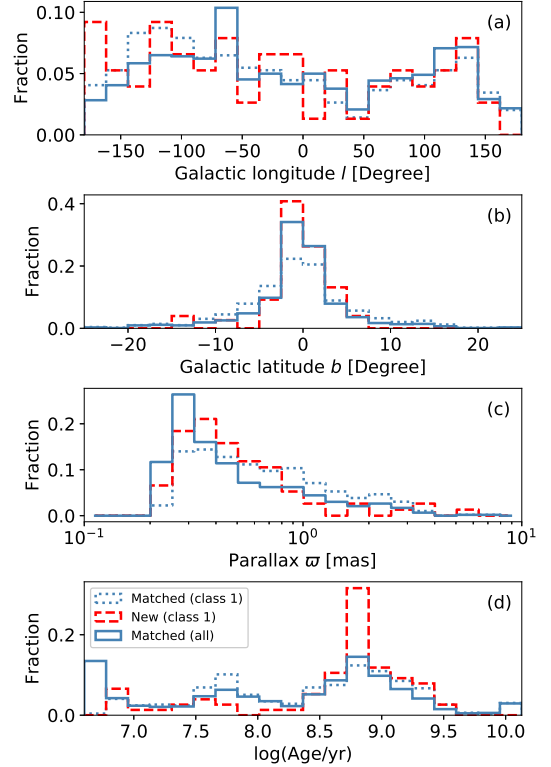
**Figure 9.** The distribution of star cluster candidates classified as Class 1 in Galactic coordinates. Blue crosses and red dots correspond to the cross-matched and newly identified star cluster candidates, respectively.



ters in Class 1 (see Tab. 3 for a full list). These previously uncataloged candidates are very likely genuine star clusters. Fig. 8 and Fig. 9 demonstrate the spatial distribution of cross-matched clusters in Class 1 (blue dots and crosses) and new star cluster candidates (red dots) in Galactic coordinates, which indicates a disk concentration for both groups, spreading out in the inter-arm regions (Fig. 8). It is necessary to carry out a systematic study to investigate the general properties of new cluster candidates, in particular their differences from known star clusters cross-matched with the catalogs of K13, CG18+19, and B19. As can be seen in Fig. 10 (panels a, b, and c), there is no major difference between the new cluster candidates and the cross-matched ones (Class 1 and all classes) in Galactic longitude, latitude and parallax. All of these are distributed mainly within  $|b| \sim 10^\circ$ . Both the cross-matched and new cluster candidates show an old population peaked at  $\log(\text{age}/\text{yr}) \sim 8.8$ . However, the excess of old star clusters is more prominent among the newly identified candidates.

#### 4.4. Candidates of cluster groups

**Figure 10.** The distributions of the Galactic longitude ( $l$ ) and latitude ( $b$ ), parallax ( $\varpi$ ) and age (derived using isochrone fitting) of all matched (blue histograms), matched Class 1 (blue dotted histograms) with K13, CG18+19 and B19, and new star cluster candidates (red dashed histograms) from Class 1.



Studies of clustering among OCs provide keys to understanding star formation in the Galactic disk and the subsequent dynamical evolution of star clusters. We carry out a search for OC groups using the FoF method amongst the clusters in our catalog (Table 1). The pro-

**Table 4.** The 56 cluster groups identified in our catalog, see data/group folder in the github repository for a full version.

Group ID	FoF ID	$l$	$b$	$\varpi$
		(deg)	(deg)	(mas)
0	30	236.057	-4.639	0.569
	51	238.210	-3.327	0.563
1	2088	265.114	-2.573	0.506
	58	264.972	-2.881	0.524
	105	264.190	-1.572	0.486
	2087	266.363	-1.917	0.476
2	1235	27.797	-1.492	0.469
	155	27.306	-2.778	0.453
3	171	120.315	-2.547	0.507
	894	121.982	-2.676	0.496
	680	120.136	-4.820	0.502
4	936	235.366	0.153	0.307
	198	234.945	-1.276	0.310
5	422	299.728	0.844	0.493
	251	299.034	-0.348	0.500
6	358	120.778	-0.953	0.320
	1321	120.355	-0.371	0.327
7	425	303.206	2.497	0.469
	2153	300.951	1.228	0.466
8	496	73.236	1.263	0.510
	493	72.653	2.067	0.522
9	1819	112.741	0.883	0.581
	526	112.808	0.430	0.595

cedure to identify these OC groups is summarized as follows:

- Since Class 1 cluster candidates are mostly at nearby clusters with good photometry, we only search for groups among the Class 1 candidates in our catalog.
- We convert the coordinates and parallaxes of selected star cluster candidates to 3-D Cartesian coordinates.
- We carry out a standard FoF group identification with a linking length of 100 pc (Conrad et al. 2017).

Conrad et al. (2017) have carried out FoF search for cluster groups in the 6-D parameter space (3-D position and 3-D velocity). Unlike in Conrad et al. (2017), radial velocities are not taken into account in our current catalog, our search of cluster groups is based on the star clusters' 3-D positions only. In total, we identify 152 star cluster candidates distributed amongst 56 cluster groups (See Tab. 4). We plot our group candidates in the Galactic X-Y plane as black triangles in Fig. 8. These group candidates are mainly concentrated in the Solar neighborhood, within distances 2 kpc, between the Perseus and Sagittarius arms. Some group candidates

only contain two star clusters, and may be candidates of binary cluster (see, e.g., Priyatikanto et al. 2016). However, kinematic data including a sufficient number of stars with radial velocities are required to confirm the dynamical status of these OC group candidates.

## 5. SUMMARY

In this work, we identify star clusters in the Milky Way disk from *Gaia* DR2 data with the Star cluster Hunting Pipeline, SHiP. Our main results are summarized as follows:

- Star clusters are identified with our FoF cluster finder in the 5-D parameter space composed of the position, parallax and proper motion. They are further verified with an isochrone fitting scheme. We classify star cluster candidates into 3 classes based on four parameters:  $\bar{d}^2$ ,  $r_n$ ,  $n_{G<17}$ ,  $t_{\text{age}}$ . SHiP is designed in a highly parallel and automated way, which makes it possible to identify star clusters in *Gaia* DR2 without any prior information.
- In total, 2443 star cluster candidates are detected, which are classified into 3 classes (with 569, 127 and 1747 cluster candidates in Class 1, 2 and 3, respectively). In our classification scheme, those classified as Class 1 are likely star clusters, showing a narrow MS in the CMD and concentration in spatial and proper motion distributions. Class 1 and 2 clusters are located at distances mainly within 4 kpc, due to the imposed constraint  $n_{G<17}$ .
- A total of 902, 714 and 876 star clusters candidates in our catalog are cross-matched with K13, CG18+19 and B19, respectively. Our star cluster catalog (Tab. 1) is in a good agreement with previously published catalogs. The discrepancies of proper motion and parallax of the matched clusters with CG18+19 are well within observational uncertainties.
- A total of 76 new star cluster candidates are detected in Class 1. These were not present in any of the earlier three catalogs. These new star cluster candidates are concentrated towards the very thin disk ( $|b| < 5^\circ$ ). The majority of these are clusters older than  $\log(\text{age}/\text{yr}) = 8.0$  with prominent narrow MSs.
- 56 candidates of star cluster group are identified by the FoF group finder based on star clusters' 3-D positions. They are distributed within 2 kpc of the Sun, between the Perseus and Sagittarius

spiral arms. Further investigations are necessary to confirm the nature of these group candidates.

The new star cluster candidates found in this work suggest that the current star cluster catalogs in the Milky Way are still incomplete. All the necessary materials, including the pipeline, catalog, 4-panel figures (including position, proper motion, parallax and CMD), member list of each individual star cluster candidate, star-cluster-group candidates, are available in the github repository: [https://github.com/liulei/gaia\\_ship](https://github.com/liulei/gaia_ship).

The authors are grateful for the financial support from the National Natural Science Foundation of China

through grants, No. 11903067, 11673032, 11503015 and U1938114. X.Y.P. expresses gratitude for support from the Research Development Fund of Xi'an Jiaotong Liverpool University (RDF-18-02-32). This study was supported by Sonderforschungsbereich SFB 881 The Milky Way System (sub-project B5) of the German Research Foundation (DFG). We thank the referee for his/her suggestions which greatly helped to improve the quality of this paper. We are also grateful to Dr. Thijs Kouwenhoven for in-depth discussions.

## REFERENCES

- Bica, E., Pavani, D. B., Bonatto, C. J., et al. 2019, *AJ*, 157, 12
- Bonatto, C. 2019, *MNRAS*, 483, 2758
- Bonatto, C., & Bica, E. 2011, *MNRAS*, 415, 2827
- Bonatto, C., Kerber, L. O., Bica, E., et al. 2006, *A&A*, 446, 121
- Cantat-Gaudin, T., Jordi, C., Vallenari, A., et al. 2018, *A&A*, 618, A93.
- Cantat-Gaudin, T., Krone-Martins, A., Sedaghat, N., et al. 2019, *A&A*, 624, A126.
- Castro-Ginard, A., Jordi, C., Luri, X., et al. 2018, *A&A*, 618, A59.
- Castro-Ginard, A., Jordi, C., Luri, X., et al. 2019, *A&A*, 627, A35
- Chabrier, G. 2001, *ApJ*, 554, 1274.
- Conrad, C., Scholz, R.-D., Kharchenko, N. V., et al. 2017, *A&A*, 600, A106
- Davis, M., Efstathiou, G., Frenk, C. S., et al. 1985, *ApJ*, 292, 371.
- Dias, W. S., Alessi, B. S., Moitinho, A., et al. 2002, *A&A*, 389, 871.
- Dieball, A., Müller, H., & Grebel, E. K. 2002, *A&A*, 391, 547
- Evans, D. W., Riello, M., De Angeli, F., et al. 2018, *A&A*, 616, A4.
- Gaia Collaboration, Brown, A. G. A., Vallenari, A., et al. 2018, *A&A*, 616, A1
- Gravity Collaboration, Abuter, R., Amorim, A., et al. 2019, *A&A*, 625, L10
- Kharchenko, N. V., Piskunov, A. E., Schilbach, E., et al. 2012, *A&A*, 543, A156.
- Kharchenko, N. V., Piskunov, A. E., Schilbach, E., et al. 2013, *A&A*, 558, A53
- Kruijssen, J. M. D. 2012, *MNRAS*, 426, 3008
- Lada, C. J., & Lada, E. A. 2003, *ARA&A*, 41, 57.
- Lindegren, L., Hernández, J., Bombrun, A., et al. 2018, *A&A*, 616, A2
- Marigo, P., Girardi, L., Bressan, A., et al. 2017, *ApJ*, 835, 77
- Meingast, S., & Alves, J. 2019, *A&A*, 621, L3
- Nelder, J. A. & Mead, R. 1965, *Computer Journal*, 7, 308
- Pang, X., Shen, S., & Shao, Z. 2018, *ApJL*, 868, L9
- Perren, G. I., Vázquez, R. A., & Piatti, A. E. 2015, *A&A*, 576, A6
- Piskunov, A. E., Schilbach, E., Kharchenko, N. V., et al. 2008, *A&A*, 477, 165
- Portegies Zwart, S. F., McMillan, S. L. W., & Gieles, M. 2010, *ARA&A*, 48, 431.
- Priyatikanto, R., Kouwenhoven, M. B. N., Arifyanto, M. I., et al. 2016, *MNRAS*, 457, 1339
- Reid, M. J., Menten, K. M., Brunthaler, A., et al. 2014, *ApJ*, 783, 130
- Röser, S., Demleitner, M., & Schilbach, E. 2010, *AJ*, 139, 2440
- Röser, S., Schilbach, E., & Goldman, B. 2019, *A&A*, 621, L2
- Springel, V. 2005, *MNRAS*, 364, 1105.
- Spitzer, L., Jr. 1958, *ApJ*, 127, 17
- Springel, V., White, S. D. M., Tormen, G., et al. 2001, *MNRAS*, 328, 726.
- Yang, X., Mo, H. J., van den Bosch, F. C., et al. 2005, *MNRAS*, 356, 1293.
- Yang, X., Mo, H. J., van den Bosch, F. C., et al. 2007, *ApJ*, 671, 153.
- Yang, S.-C., Sarajedini, A., Deliyannis, C. P., et al. 2013, *ApJ*, 762, 3